

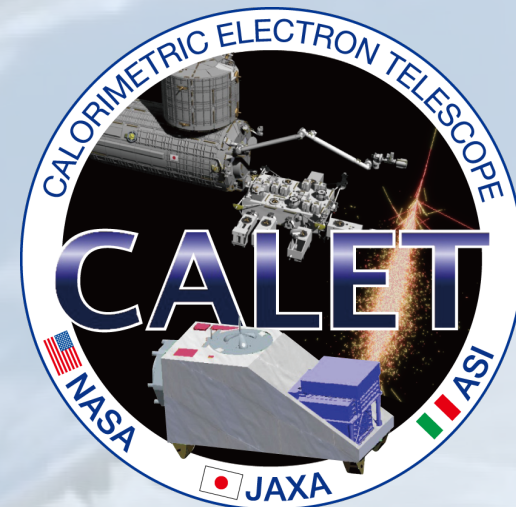


SH #332

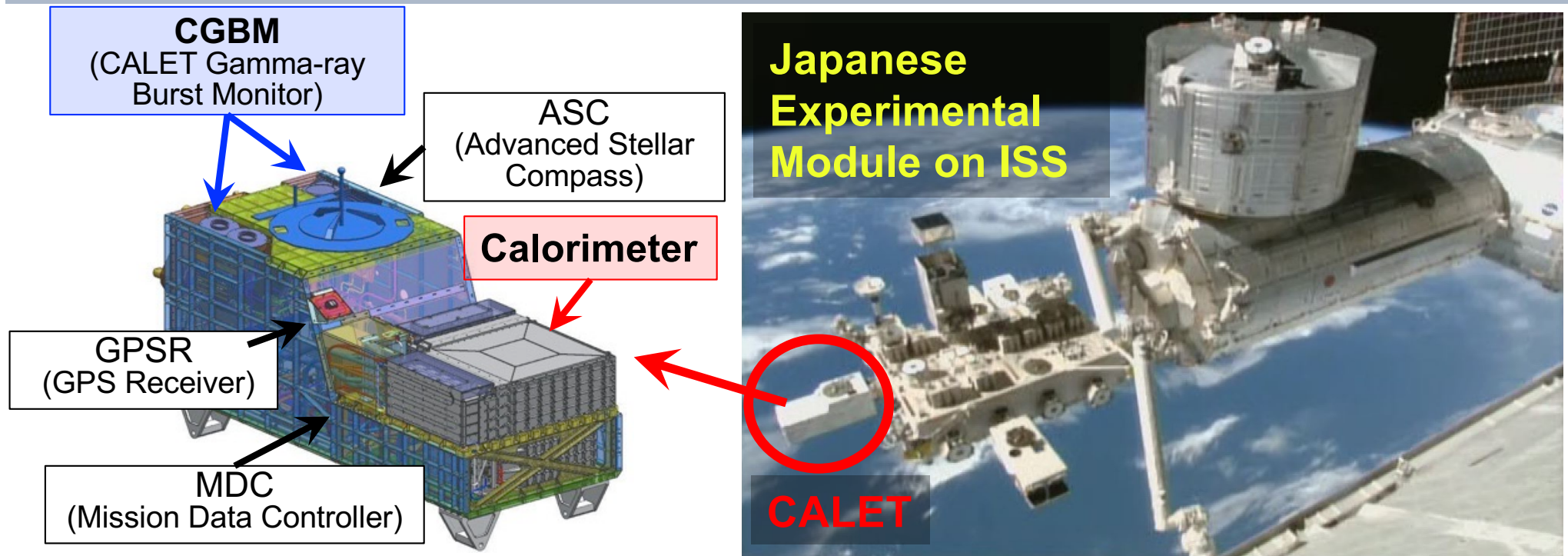
Solar Modulation During the Descending Phase of Solar Cycle 24 Observed with CALET on the International Space Station

S. Miyake for the CALET Collaboration

National Institute of Technology(KOSEN), Ibaraki College



CALorimetric Electron Telescope (CALET)



Launch: Aug. 19, 2015

Start of Nominal Observations: Oct. 13, 2015

Observation Targets:

Electron ($e^- + e^+$): 1 GeV – 20 TeV

p--Fe: 10 GeV – 1000 TeV

Ultra heavy ions ($26 < Z \leq 40$): > 600 MeV/n

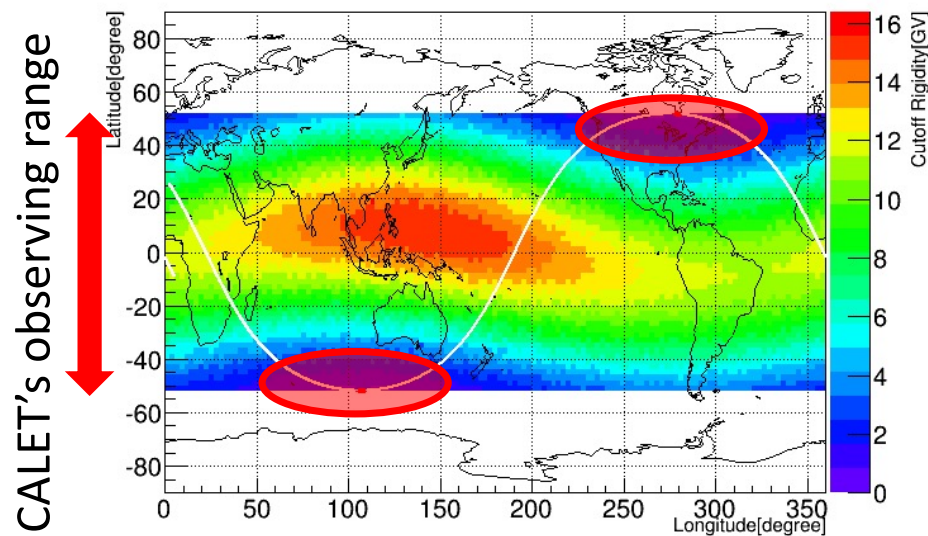
Gamma-rays (Diffuse + Point sources): 1 GeV – 1 TeV

Measurements of low-energy CR $e^- + e^+$ with CALET

Low-Energy Electron shower trigger (LEE-Trigger):

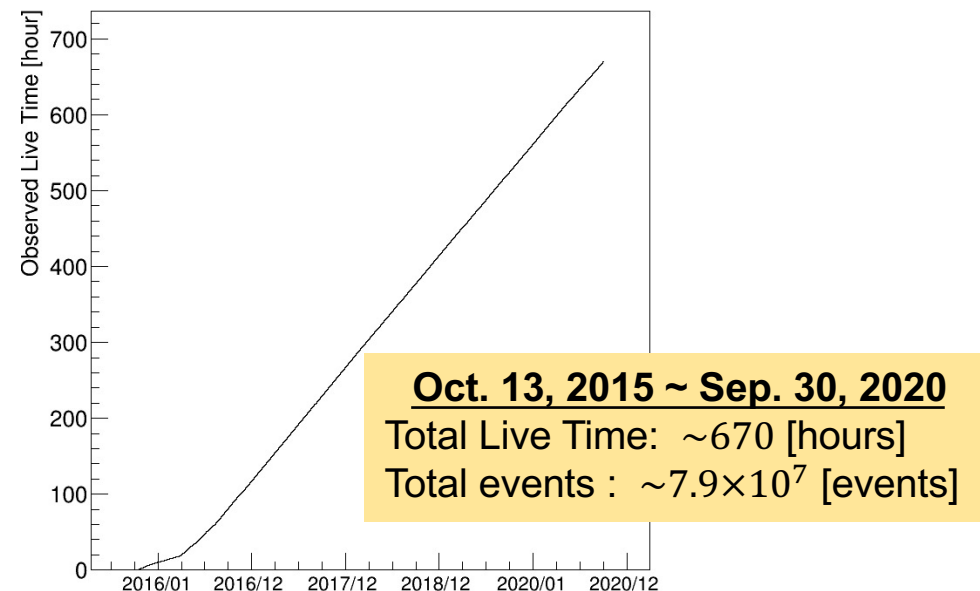
- Energy thresholds are set to detect shower events with energies above 1.0 GeV.
- Measurement of low energy electrons (1GeV ~ 10GeV) with LEE-trigger is applied only at high latitude where maximum cutoff rigidity is 5.0GV.
 - In 1 cycle (~90 min.), the LEE trigger mode works 2 times for 90 sec in northmost and southmost region on the orbit.

Cutoff rigidity map and ISS orbit



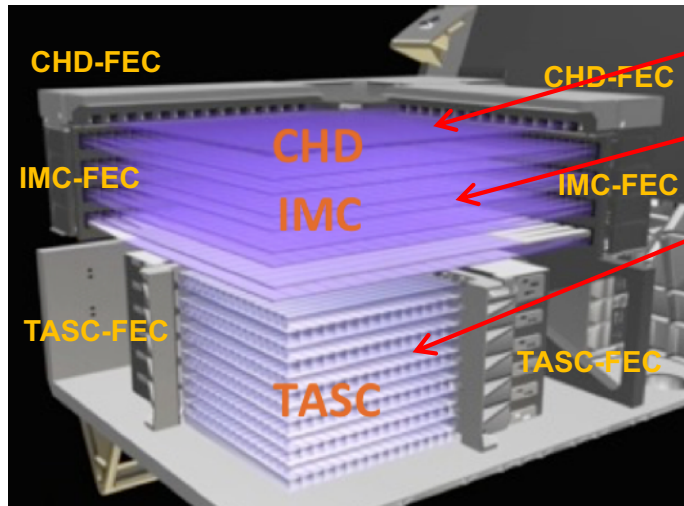
<http://www.ngdc.noaa.gov/AGA/vmod/igrf.html>

Integrated live time



Analysis Procedure for Low-Energy $e^- + e^+$

CALET calorimeter



CHD (Charge Detector)

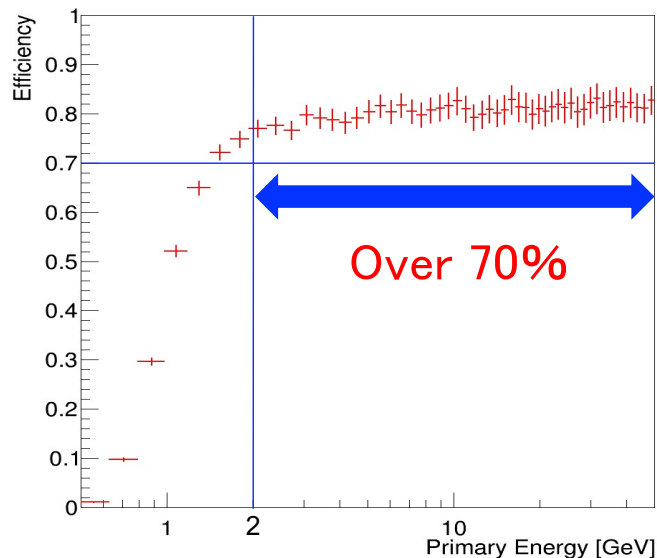
IMC (Imaging Calorimeter)

TASC (Total Absorption Calorimeter)

Event selections for low energy $e^- + e^+$

- ① Energy threshold: **IMC7-8 and TASC top layer**
 - Trigger GeV-energy events
- ② Tracking and geometry condition: **IMC**
 - Kalman filter track reconstruction with IMC
 - Entire trajectory is inside IMC and TASC
- ③ Charge determination: **CHD**
 - CHD energy deposit to remove $Z \geq 2$
- ④ e/p separation: **IMC bottom layer and TASC top layer**
 - Energy deposit and Shower concentration of IMC bottom layer
 - R_E of TASC top layer
- ⑤ Energy determination: **IMC and top 3 layers of TASC X, Y**
 - Energy deposit of top 3 layers of TASC X, Y and IMC

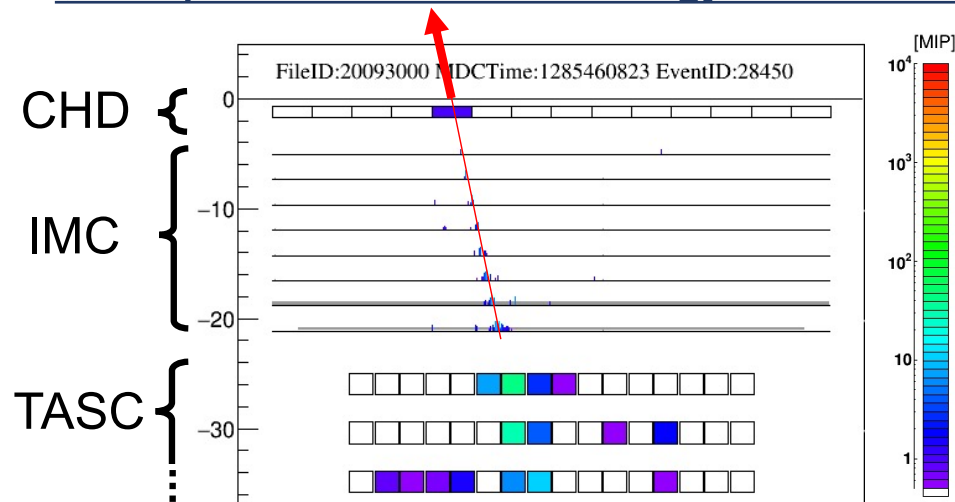
Energy dependence of low-energy $e^- + e^+$ Efficiency



Geomagnetic Cutoff Rigidity

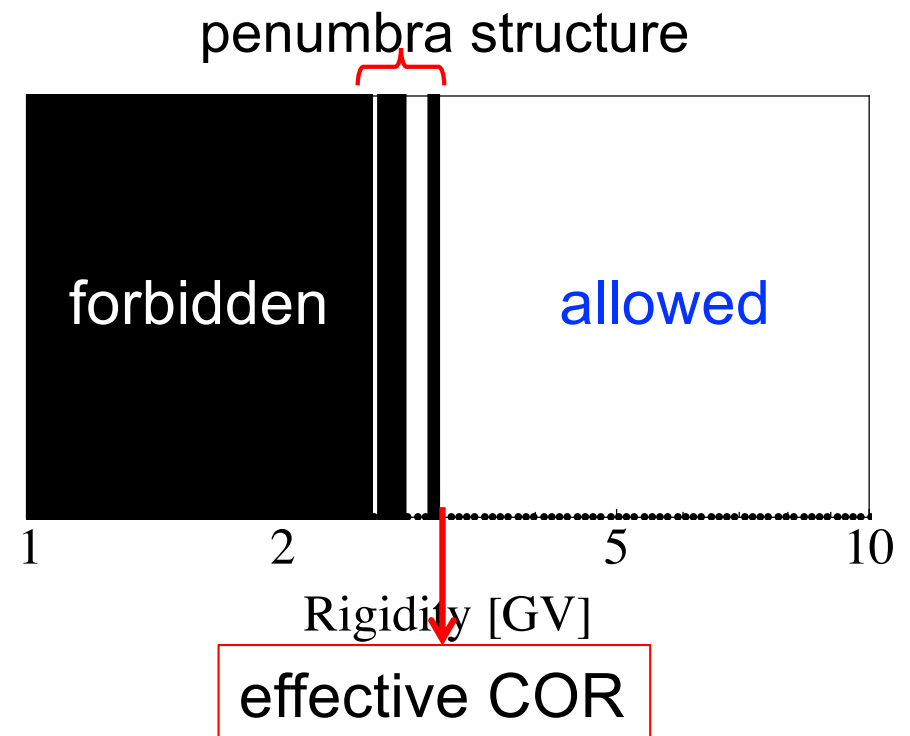
- We have calculated the effective cutoff rigidity by reconstructing particle trajectories in the magnetosphere, implementing a realistic description of the geomagnetic field based on the IGRF-13 and TS05 empirical models.
- A direction of each incident particle has been set to the reconstructed trajectory with CHD and IMC.
- To select events that are not affected by the geomagnetic cutoff, we have defined the effective cutoff rigidity as the lowest rigidity in which a penumbra structure does not appear.

Direction of the particle trajectory for the back-tracing calculation in the magnetosphere (example of events with energy of 4.4 GeV)



(A posture of the calorimeter in the GSE coordinate is also considered.)

Definition of the effective cutoff rigidity

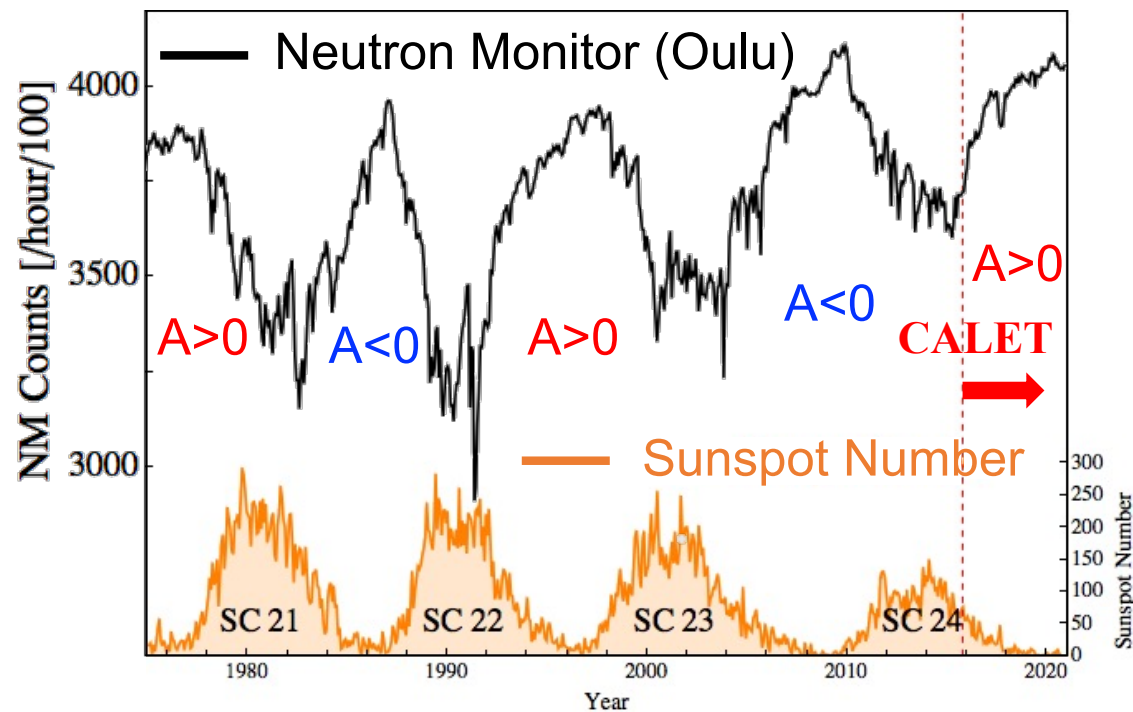


Motivation of the Observation of the Solar Modulation

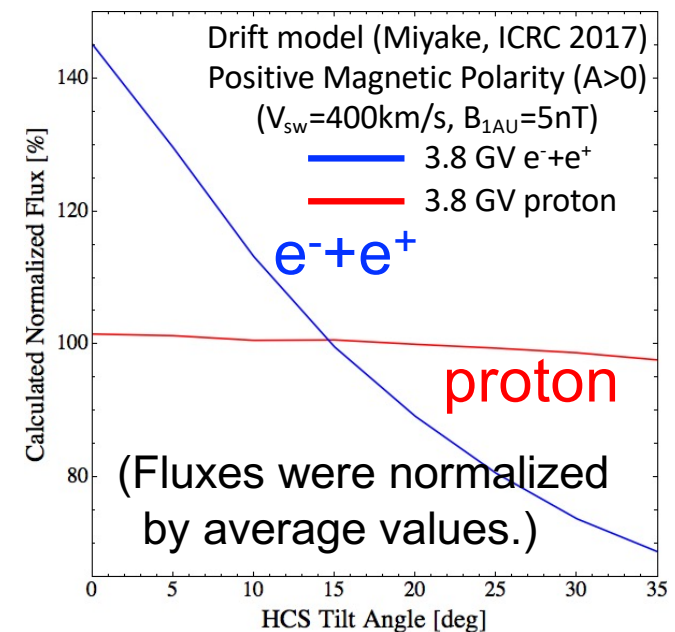
The solar modulation has a charge sign dependence by the product qA of the magnetic field polarity A and the CR's charge q .

- Owing to the weak solar cycle activity and the qA negative polarity for electrons, the highest electron flux in observation history may be detected during the solar minimum.
- The charge sign dependence of solar modulation can be investigated by comparing the solar modulation of protons and electrons.

22-years variations of the solar modulation



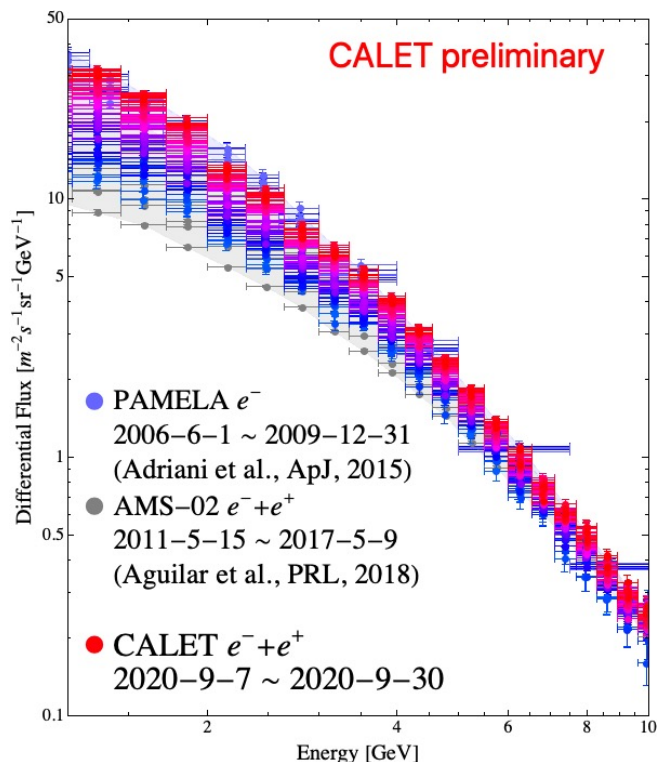
Charge sign dependence expected from the drift model of the solar modulation



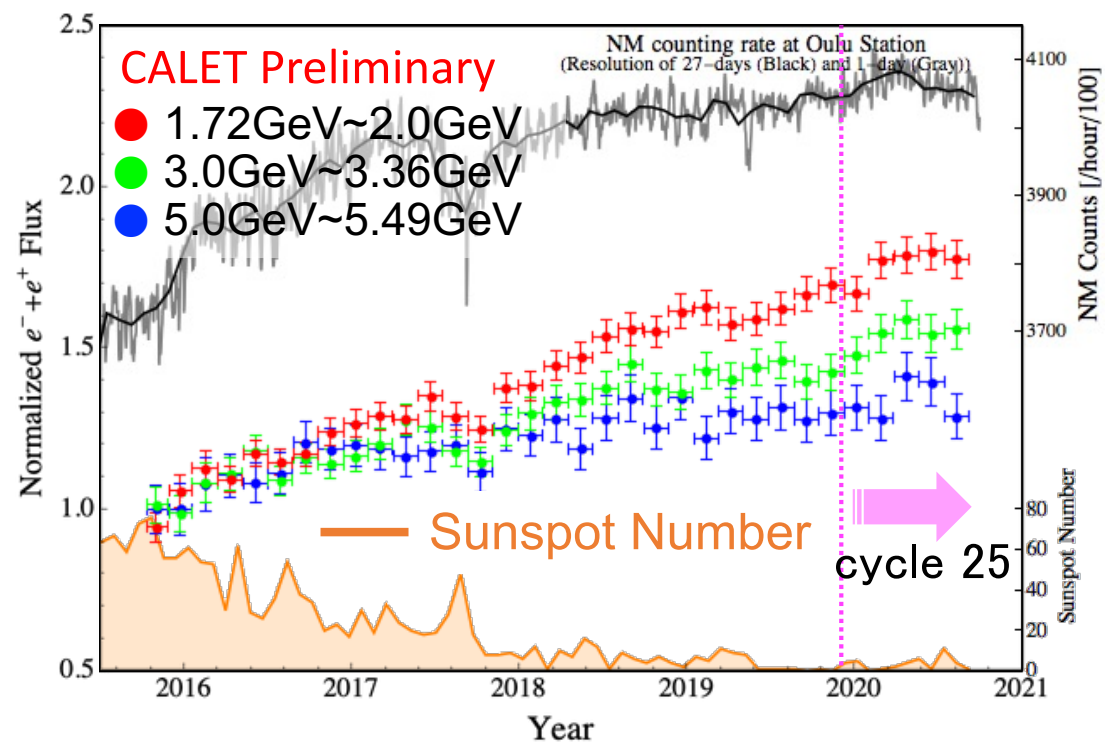
Long-Term Variation of the CR $e^- + e^+$ Flux

- The electron flux in the 1-10 GeV region has been continuously increased until about half a year after beginning the new solar cycle.
- The flux during the solar minimum has reached to the maximum, which is comparable or exceeded the maximum flux observed with PAMELA in last solar minimum period.
- The flux has begun to decrease.

CR $e^- + e^+$ energy spectrum



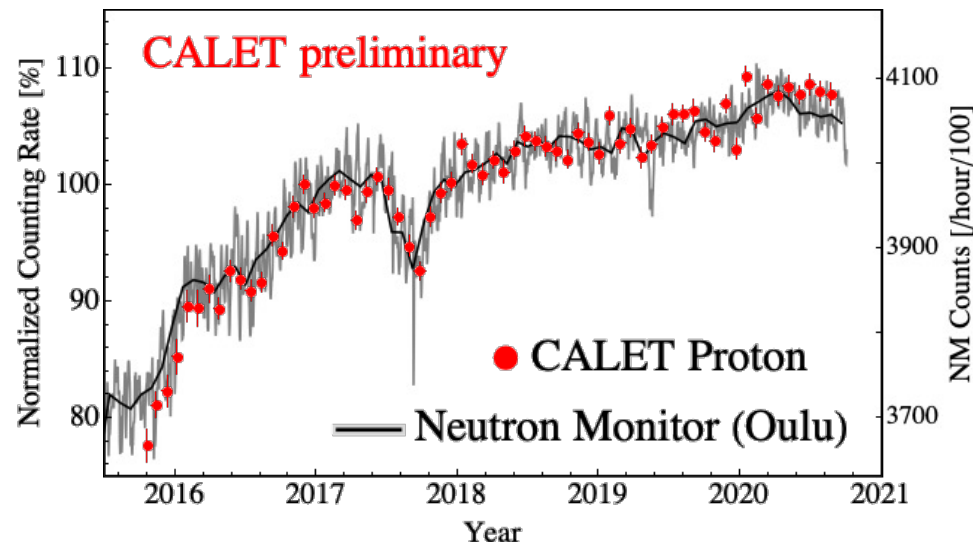
Time profile of the flux



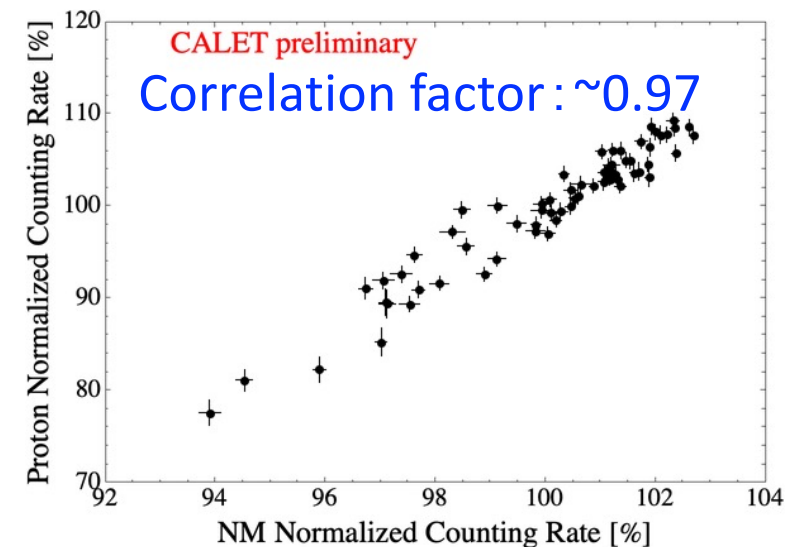
Normalized Count Rate of CR protons

- We have analyzed the count rate of low-energy protons of which the mean rigidity is adjusted to be ~ 3.8 GV that is the mean rigidity of the count rate of electrons.
- We have selected events that has detected in the region where the cutoff rigidity is under 1.2GV.
- The count rate of CR protons also increases with decrease of the solar activity level, which has a strong correlation with the count rate of a neutron monitor observed at low geomagnetic cutoff.

Time profile of the count rate of CR protons and that of neutron monitor



Correlation with count rate of CR protons and that of neutron monitor

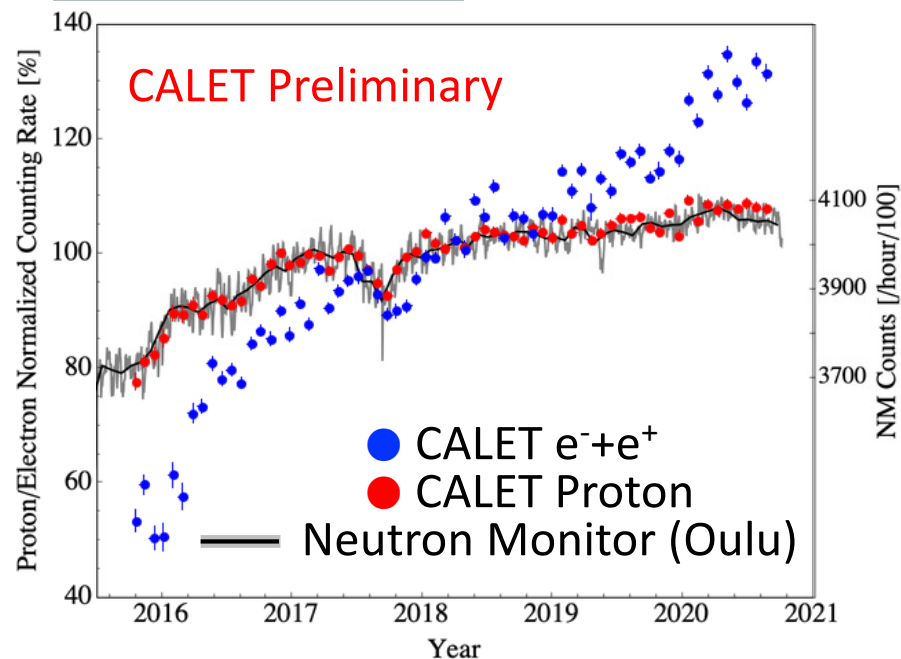


(Count rate of protons and that of neutron monitor are normalized with each average value.)

Normalized Count Rate of CR protons and $e^+ + e^-$

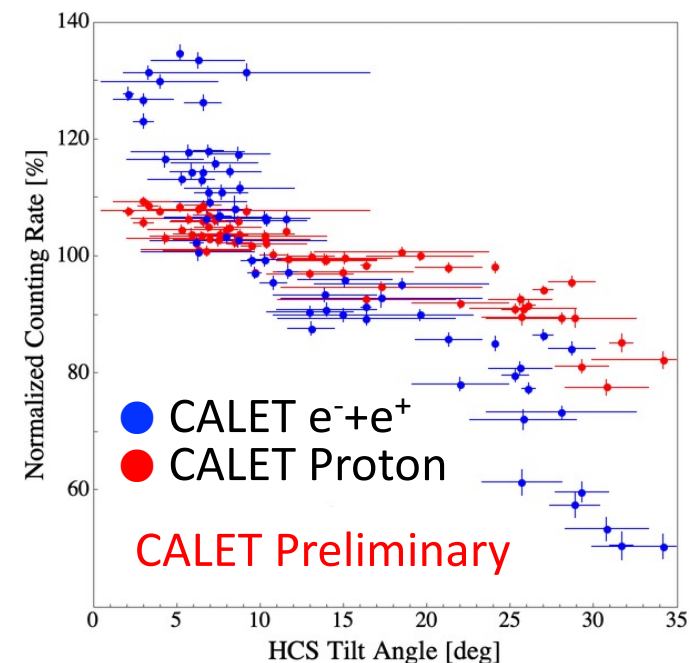
- To investigate the charge sign dependence of the solar modulation, we have evaluated the count rate of CR $e^- + e^+$ in which the average rigidity is the same as that of count rate of CR protons.
- We have found the variation range of the count rate of CR $e^- + e^+$ is clearly larger than that of CR protons. The observed results are consistent with the charge sign dependence expected from the drift model of the solar modulation.

Time profile of the count rate of CR protons and $e^- + e^+$



(Each count rate is normalized with each average value.)

Correlation with count rate of CR protons/ $e^- + e^+$ and HCS tilt angle



Summary

- The $e^- + e^+$ flux observed by CALET in the 1-10 GeV region during the solar minimum has reached its maximum in 2020, which is comparable or exceeded the maximum flux observed with PAMELA in the last solar minimum period.
- The count rate of CR protons also increases with decrease of the solar activity level, which has a strong correlation with the count rate of a neutron monitor observed at low geomagnetic cutoff.
- We have found the variation range of the count rate of CR $e^- + e^+$ is clearly larger than that of CR protons. The charge sign dependence is consistent with that expected from the drift model of the solar modulation.